Cardiovascular Research (2012) **95**, 469–479
doi:10.1093/cvr/cvs210

The effect of connexin40 deficiency on ventricular conduction system function during development

Barbora Sankova[1,2†], Jiri Benes Jr[1,2†], Eliska Krejci[1,2], Laurent Dupays[3], Magali Theveniau-Ruissy[4], Lucile Miquerol[4], and David Sedmera[1,2*]

[1]Department of Cardiovascular Morphogenesis, Institute of Physiology, Academy of Sciences of the Czech Republic, Videnska 1083, 14220 Prague, Czech Republic; [2]First Faculty of Medicine, Institute of Anatomy, Charles University in Prague, Prague, Czech Republic; [3]Division of Developmental Biology, MRC National Institute for Medical Research, Mill Hill, London, UK; and [4]Developmental Biology Institute of Marseilles-Luminy (IBDML), CNRS UMR7288 Aix-Marseille Université, Campus de Luminy, Marseille, France

Received 29 November 2011; revised 19 June 2012; accepted 21 June 2012; online publish-ahead-of-print 27 June 2012

Time for primary review: 16 days

Aims The aim of this study was to characterize ventricular activation patterns in normal and connexin40-deficient mice in order to dissect the role of connexin40 in developing the conduction system.

Methods and results We performed optical mapping of epicardial activation between ED9.5–18.5 and analysed ventricular activation patterns and times of left ventricular activation. Mouse embryos deficient for connexin40 were compared with normal and heterozygous littermates. Morphology of the primary interventricular ring (PIR) was delineated with the help of T3-LacZ transgene. Four major types of ventricular activation patterns characterized by primary breakthrough in different parts of the heart were detected during development: PIR, left ventricular apex, right ventricular apex, and dual right and left ventricular apices. Activation through PIR was frequently present at the early stages until ED12.5. From ED14.5, the majority of hearts showed dual left and right apical breakthrough, suggesting functionality of both bundle branches. Connexin40-deficient embryos showed initially a delay in left bundle branch function, but the right bundle branch block, previously described in the adults, was not detected in ED14.5 embryos and appeared only gradually with 80% penetrance at ED18.5.

Conclusion The switch of function from the early PIR conduction pathway to the mature apex to base activation is dependent upon upregulation of connexin40 expression in the ventricular trabeculae. The early function of right bundle branch does not depend on connexin40. Quantitative analysis of normal mouse embryonic ventricular conduction patterns will be useful for interpretation of effects of mutations affecting the function of the cardiac conduction system.

Keywords Mouse embryo • Right bundle branch block • Left bundle branch • Optical mapping

1. Introduction

The mouse is a popular genetic model for human diseases, including those of the cardiovascular system. Some of these involve the normal function of the cardiac conduction system. Despite its morphology being well characterized down to the molecular level, a comprehensive quantitative study of conduction system function is not available.

Extensive studies in the chick embryo[1–4] have shown that the hallmark of ventricular conduction system function is the shift of ventricular activation to a pattern originating from the apex, rather than the base of the heart. Before this shift, the activation pattern utilizes a preferential pathway along forming the interventricular septum known as the primary interventricular ring (PIR).[5] The term 'primary ring' was first used by Wessels *et al.*;[6] the PIR represents only the ventricular part of this structure described in preseptated mouse and human hearts. It connects proximally to the ring-shaped atrioventricular canal, which acts as a delay generator prior to differentiation of the atrioventricular node. During further morphogenesis, rightward expansion of the atrioventricular canal that creates the inflow to the right ventricle results in opening of the PIR, transforming it into a horseshoe-shaped structure.[5] In the chick, the mature activation pattern is already observed during chamber formation, but becomes fully established only after ventricular septation. In contrast, studies in the embryonic mouse[7,8] and rabbit[9] suggested that apex-to-base activation is present from the onset of chamber formation in mammals. Our data from embryonic rats,[10] however, have

† B.S. and J.B. contributed equally to this manuscript.

* Corresponding author. Tel: +420 296 442 561; fax: +420 241 062 488, Email: dsedmera@biomed.cas.cz

shown rather diffuse epicardial breakthrough at early stages as well as a base-to-apex preferential conduction pathway along the forming interventricular septum. Since all the mammalian studies are based on a rather small number of analysed hearts, we felt that a systematic, quantitative overview of mouse embryonic activation patterns was due, and would likely uncover similar variability, as did our earlier chicken studies.

Conduction through the cardiac tissue is determined by the tissue geometry (cell size and shape, intercellular connections, and amount and distribution of connective tissue) as well as by ion channels expression and type together with the polarity of the intercellular junctions. One important determinant of conduction velocity and anisotropy is the expression and the distribution of gap junction (gj) proteins—connexins. Five major connexins (Cx) are expressed in the mouse heart in dynamic spatiotemporal patterns. Cx45 (gja7) is expressed at low levels throughout the myocardium and is enriched in the slow-conducting nodes and the extended cardiac conduction system.[11,12] Its deletion results in early lethality and conduction block. The recently identified Cx30.2 (gjd3) is also characteristic of the slowly conducting areas.[13] Cx30 (gjb6) is specifically expressed in a part of the sinoatrial node, and modulates the intrinsic heart rate.[14] Cx43 (gja1) is the main connexin of the working chamber myocardium, and its deficiency results in slower conduction and a propensity for arrhythmias.[15–17] Cx40 (gja5) is expressed in the mouse embryo in the fast-conducting atrial myocardium and ventricular chamber myocardium; there, it becomes gradually restricted to the entire trabecular network and subsequently to the bundle branches and the Purkinje fibre network.[18–20] Cx40 deficiency causes embryonic and atrial conduction anomalies[21] and slower conduction with right bundle branch block in the ventricular conduction system.[22–25] However, the functional importance of Cx40 in the developing conduction system has not been studied.

The first aim of this study was thus to characterize the major ventricular activation patterns during mouse development and correlate them with cardiac morphogenesis and conduction system formation. The second goal was to assess the effects of a lack of Cx40, considered to be a robust marker of the ventricular conduction system, on conduction system function during development.

2. Methods

2.1 Animals

All the animal experiments were performed in accordance with the Czech law governing animal care and experimentation, and were approved by the institutional committee. The investigation conforms to the European Directive 2010/63/EU of the European Parliament. The Cx40:GFP knock-in mice were described previously.[18] They were maintained in a homozygous state and crossed with the Swiss strain. The breeding pairs set up to obtain the desired embryonic genotypes (wild type, heterozygous, and homozygous) were caged overnight and the noon of the day when plug was discovered was considered embryonic day (ED) 0.5. Time-pregnant females (ED9.5–18.5) were killed by cervical dislocation and the embryos rapidly dissected in cold Tyrodes-HEPES solution (pH 7.4). In total, 397 embryos were analysed, with a minimum of two litters and 10 embryos per genotype per stage.

2.2 Optical mapping

The embryos were first decapitated, and the hearts together with the adjacent posterior thoracic wall were isolated and stained with voltage-sensitive dye di-4-ANEPPS for 5–15 min (depending on the stage) in preparation for optical mapping exactly as described recently.[5] The only difference was the addition of blebbistatin[26,27] into the staining solution for the hearts at ED16.5 and 18.5 to shorten the equilibration period in warm oxygenated Tyrodes during which the hearts became frequently arrhythmic. Analysis of recordings resulting in the generation of spatiotemporal epicardial activation maps was performed using the BV_Analyzer software bundled with the Ultima L camera as described previously.[28,29] In-depth discussion of the limitations of this approach as well as arrhythmias encountered in the embryonic hearts can be found in the Supplementary material online.

2.3 Data analysis and statistics

Ventricular activation patterns were interpreted in conjunction with morphology as discussed previously, and categorized accordingly. The differences in the frequency of the individual patterns[2] were analysed using Person's Chi-square test in Microsoft Excel, and *P*-values below 0.05 were considered significant. The differences in the continuous variable (ventricular activation times) were compared using unpaired two-tailed Student's *t*-test. The data are presented as mean ± SD.

2.4 Morphological evaluation

For the morphogenesis of the mouse ventricular conduction system, we used previously published data by Viragh and Challice,[30–32] Rentschler *et al.*,[7,8] and our own studies.[18,33] The PIR theory is supported by additional studies in humans,[6,34] chicks,[3] and rats;[10] for its visualization in the mouse, we used the T3 transgene and X-gal staining as described.[35] A 22 kb fragment of the Cx40 genomic domain was cloned and sequenced. The cloned region comprised a non-coding region with 4 kb upstream of the first non-coding exon (exon 1) plus the 18 kb intron. This fragment was engineered upstream of the nls-LacZ reporter gene, replacing the coding exon 2, and used to generate a transgenic mouse line. In addition, we analysed the extent of *Cx*40 expression by whole-mount epifluorescence and confocal microscopy.[36] For further morphological analysis, the hearts were fixed in 4% paraformaldehyde for 1 h and processed for standard paraffin histology. Serial sections were alternatively stained with haematoxylin–eosin, anti-alpha smooth muscle actin (Sigma) or anti-beta galactosidase (cappel-MP Biomedicals), and anti-TBX3 (E-20, Santa-Cruz) antibodies using standard procedures.[18] 3D images of whole-mount immunofluorescence were acquired with a two-photon microscope (Zeiss MP7) and images were treated with the Volocity software.

3. Results

3.1 Conduction at early developmental stages

The earliest time point when we were able to obtain reproducible recordings from stable hearts was ED9.5. The younger hearts showed either no spontaneous activity or complete atrioventricular block after staining, and this was not alleviated even if they were stained by the generally less toxic calcium indicator rhod-2. The embryonic heart at ED9.5 had a primitive right ventricle, less developed than the left ventricle, and *Cx*40 was expressed only in the atria, the left ventricular chamber, and the endocardium of the outflow tract (*Figure 1A*). From ED10.5, *Cx*40 expression was observed in the trabeculae of the right ventricle (*Figure 1B* and *C*). *Cx*40 was absent in the PIR tissues; these could be visualized at this stage with the T3-lacZ transgene whose expression marked a ring around the interventricular foramen (*Figure 1D–F*) best visible from the lateral view. At mid-gestation, the T3-lacZ reporter gene is expressed in the

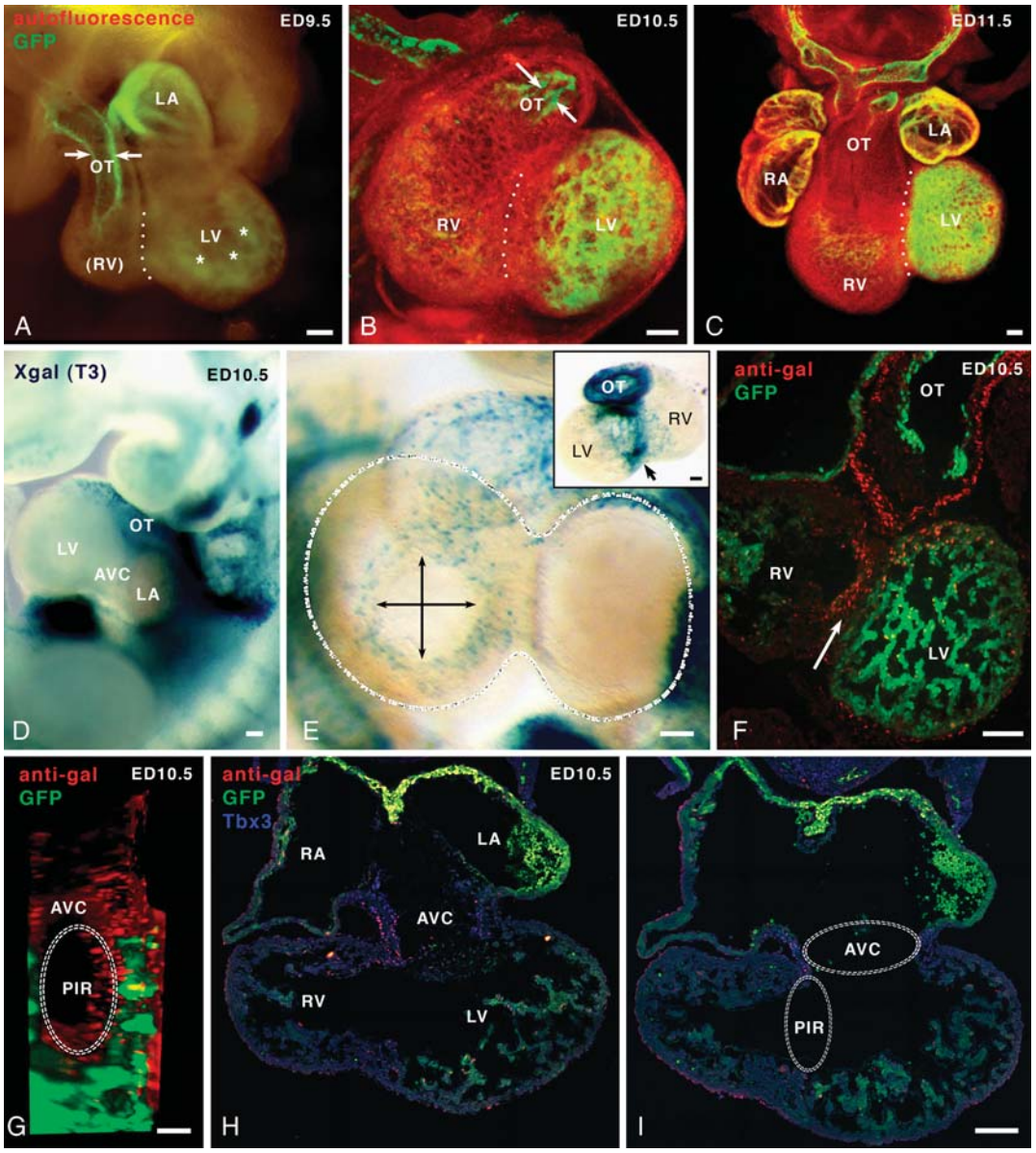

Figure 1 The morphology of the ventricular conduction system in the developing mouse heart. (*A*) *Cx*40 expression visualized by *Cx40:GFP* fluorescence at ED9.5 is found in the atria, the (left) ventricular trabeculae (asterisks), and the outflow tract endocardium (arrows). (*B*) At ED10.5, the expression is more prominent in the left ventricle, although some staining is visible in the right ventricular trabeculae as well as the outflow tract endocardium. (*C*) This pattern is similar at ED11.5, where a rich network of the pectinate muscles could be seen in both atrial appendages. White dots indicate the position of the PIR, devoid of Cx40, corresponding externally to forming interventricular groove. (*A*, *B*, *C*) Tissue autofluorescence in the red channel, in green GFP fluorescence. (*D*) T3-LacZ expression detected in whole-mount staining of an ED10.5 heart in a left lateral view and in a dorso-ventral view of the heart. The transgene is expressed in the branchial arches, the outflow tract, and the dorsal region of the atria. In addition, the transgene detects the primitive ring present as a circle at the ventricular level (*E*, higher magnification, double-sided arrows). Insert shows the same heart-posterior view in transmitted light after isolation from the embryo confirming the heavy staining in the PIR between the left and the right ventricle (arrow) and the outflow tract. (*F*) Nuclear expression of the beta galactosidase (red) is detected by immunohistochemistry on a section of an ED10.5 heart in the PIR tissues (arrow), which are devoid of Cx40 (green, detected by GFP fluorescence), as well as in the outflow tract myocardium. (*G*) Two-photon whole-mount immunoconfocal reconstruction of the PIR at ED10.5 from the lateral view. T3 transgene expression dominant in the endocardium and the epicardium is visualized in red with an antibody against beta-galactosidase, in green channel GFP (Cx40) also detected by immunohistochemistry. For more detail, see Supplementary material online, *Movie S1*. (*H*) A frontal section at ED10.5 of a T3 *Cx40:GFP* heart to illustrate the transgene expression in the atrioventricular canal and the PIR (red); in blue is the Tbx3 immunostaining. (*I*) A more posterior section of the same heart with the outlines of the PIR and the AVC, connecting at the inner curvature. Scale bars 100 μm. AVC, atrioventricular canal; Ao, aorta; LA, left atrium; LV, left ventricle; OT, outflow tract; PIR, primary interventricular ring; Pu, pulmonary trunk; RA, right atrium; RV, right ventricle.

Table 1 The frequency of epicardial activation patterns during development in *Cx40:GFP* heterozygotes

ED	PIR	LAB	RAB	LAB+RAB
9.5	10 (63%)	6 (37%)	0	0
10.5	24 (67%)	12 (33%)	0	0
11.5	7 (37%)	3 (16%)	8 (42%)	1 (5%)
12.5	1 (3%)	4 (13%)	15 (48%)	11 (36%)
13.5	0	2 (6%)	13 (41%)	17 (53%)
14.5	0	7 (28%)	3 (12%)	15 (60%)

The frequency of ventricular activation by the PIR declines between ED9.5 and 12.5, being replaced by the apex to base activation pattern. The presence of both left and right apical breakthrough was the most common pattern at ED14.5. The same frequency of ventricular activation patterns (with minor deviations) was also seen in wild types of several different backgrounds (data not shown).
PIR, primary interventricular ring; RAB, right apical breakthrough; LAB, left apical breakthrough.

myocytes of the atria and the atrio-ventricular conduction system as indicated by the Tbx3 co-staining but not in the ventricular myocardium (GFP-positive; *Figure 1H* and *I*). The three-dimensional image of the PIR (T3-lacZ-positive) demonstrated its connection to the atrioventricular ring and the *Cx*40-positive ventricular trabeculae (*Figure 1G–I*), and this can be best appreciated in the Supplementary material online, *Movie S1*. These results confirm the existence of a specific ring of cardiomyocytes (PIR) joining the atrioventricular conduction system to the conductive ventricular trabeculae.

At early developmental stages (ED9.5–10.5, *Table 1*), we observed two activation patterns using optical mapping: the first one from the primitive (left) ventricular apex, and the other, more frequent, originating from the forming interventricular (bulboventricular) groove (*Figure 2*). The electrical impulse was generated at the site of the forming sinoatrial node and spread bilaterally to both atria. From the atrioventricular canal, the electrical impulse was transmitted to the ventricles along the junction of the atrioventricular canal and the PIR (*Figure 2*). As the PIR is a circular structure, the electrical

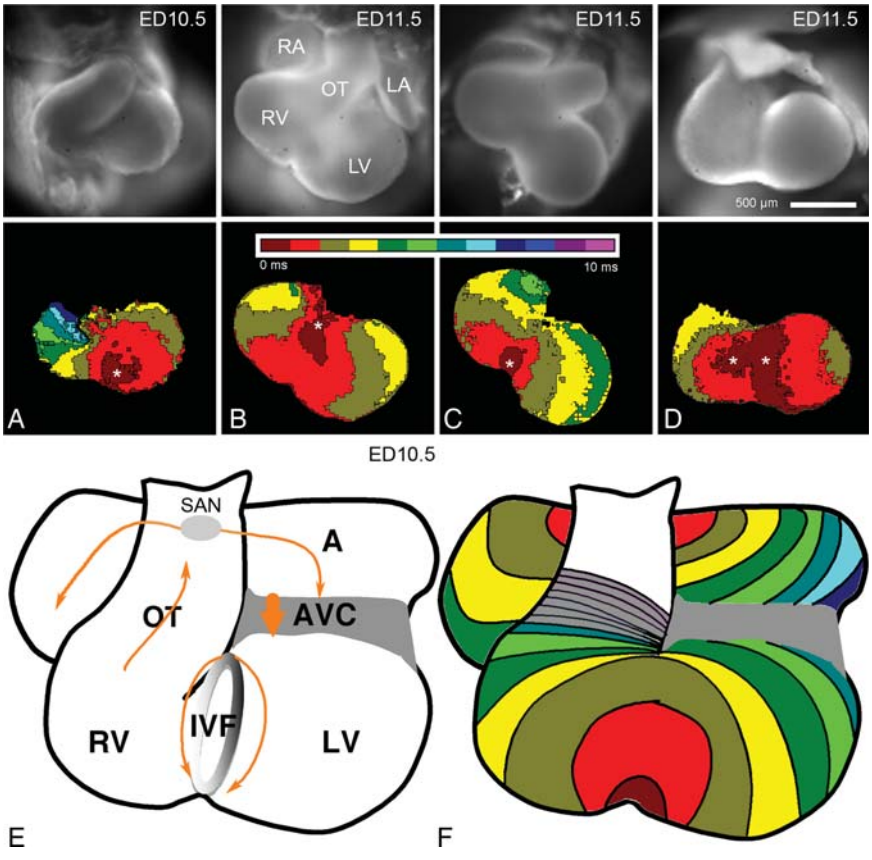

Figure 2 Examples of transitional activation patterns in early embryonic hearts. All examples are from *Cx40:GFP* heterozygous embryos; each colour band corresponds to a 1 ms time interval, and an asterisk indicates the first epicardial breakthrough site. (*A*) A single left-sided breakthrough (asterisk) at ED10.5. (*B*) The PIR type of activation at ED11.5, starting from the atrioventricular junction ventrally. (*C*) The same pattern, but using the posterior pathway, resulting in the first activation apparent ventrally in the interventricular groove between the right and left ventricular apices, was observed in a littermate of (*B*). (*D*) Transition between the ring-type and the apex-to-base activation patterns resulting in two distinct activation foci was also observed at ED11.5. (*E*) A diagram showing an ED10.5 heart and the spread of electrical impulse marked by orange arrows. (*F*) A typical epicardial activation map of an ED10.5 heart (depicted in *E*) obtained by merging atrial and ventricular activation maps. Electrical impulse is generated in the site of the sinoatrial node (SAN) and spreads laterally (atrial activation time 8 ms). The atrioventricular canal is not visualized on activation maps due to overlap with the atria, and the delay generated there is 180 ms. In this example, the ventricles are activated along the dorsal preferential activation pathway of the PIR. The outflow tract is another slowly conducting region (not coloured, isochronal intervals 1 ms). AVC, atrioventricular canal; IVF, interventricular foramen; LA, left atrium; LV, left ventricle; OT, outflow tract; RA, right atrium; RV, right ventricle.

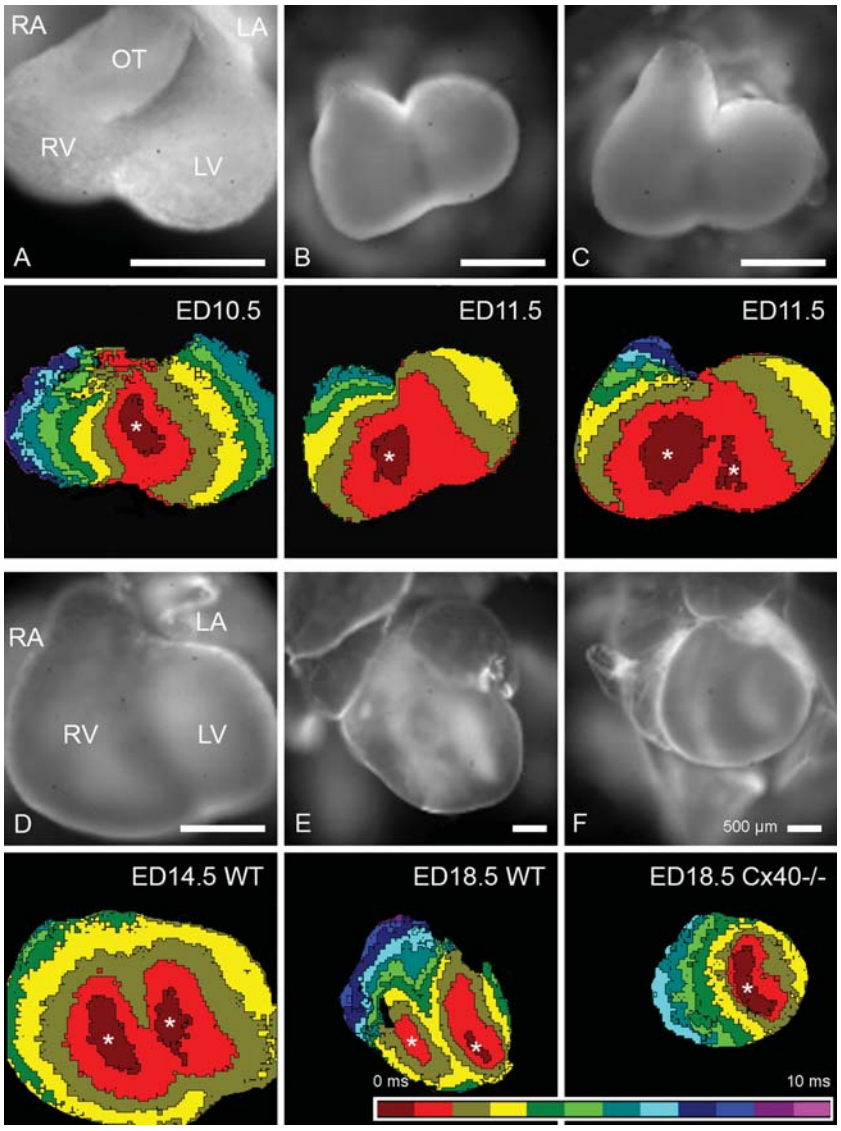

Figure 3 Typical examples of ventricular activation patterns observed in the developing mouse heart. (*A*) PIR-type activation at ED10.5. (*B*) Right-sided apical breakthrough at ED11.5. (*C*) Dual left- and right-sided breakthrough at ED11.5. All examples are from *Cx40:GFP* heterozygous animals. (*D*) Typical dual left- and right-sided apical breakthrough at ED14.5 in the wild type, interpreted as an evidence of the function of the right and left bundle branch. (*E*) The same pattern is also the most common one in the wild type at ED18.5. (*F*) A typical single (left) apical breakthrough in a *Cx*40-null heart, interpreted as right bundle block. The coloured isochrones are in 1 ms intervals and the white asterisk marks the first site of activation. The scale bars in all panels are 500 μm.

impulse travels into the ventricles along its ventral (*Figure 2B*) or dorsal aspect. The latter case was manifested as ventricular activation initiating between the apices of the ventricles (*Figure 2C*).

3.2 Conduction at later developmental stages

From ED11.5, four basic patterns of conduction, consistent with previous data from literature,[7,8] were detected (*Figure 3A–C*). Until ED12.5, the ventricles were activated through the PIR using a preferential pathway along the forming interventricular septum. The frequency of this pattern, initially present in the majority of hearts (*Table 1*), gradually decreased. Several transitional patterns were observed at ED10.5–ED11.5 (*Figure 2D*), until clear apex-to-base activation was observed, originating initially and more frequently from the right side. This right-sided breakthrough, first present at ED11.5, was observed in nearly all hearts from ED14.5, at which stage it could be related to the functionality of the right bundle branch. In addition, a second breakthrough near the left ventricular apex was observed from ED11.5. Unlike at earlier stages (ED9.5–10.5) where the single breakthrough originated exclusively from the primitive left ventricle, it was almost always present with the right-sided breakthrough (*Figure 3C* and *D*). We thus suggest that it represents activation through the emerging left bundle branch. The temporal difference between these two activation sides was minor, always below 2 ms, neither of them being consistently earlier than the other. The exception was at ED12.5, when the left breakthrough never preceded the right one in hearts showing dual activation.

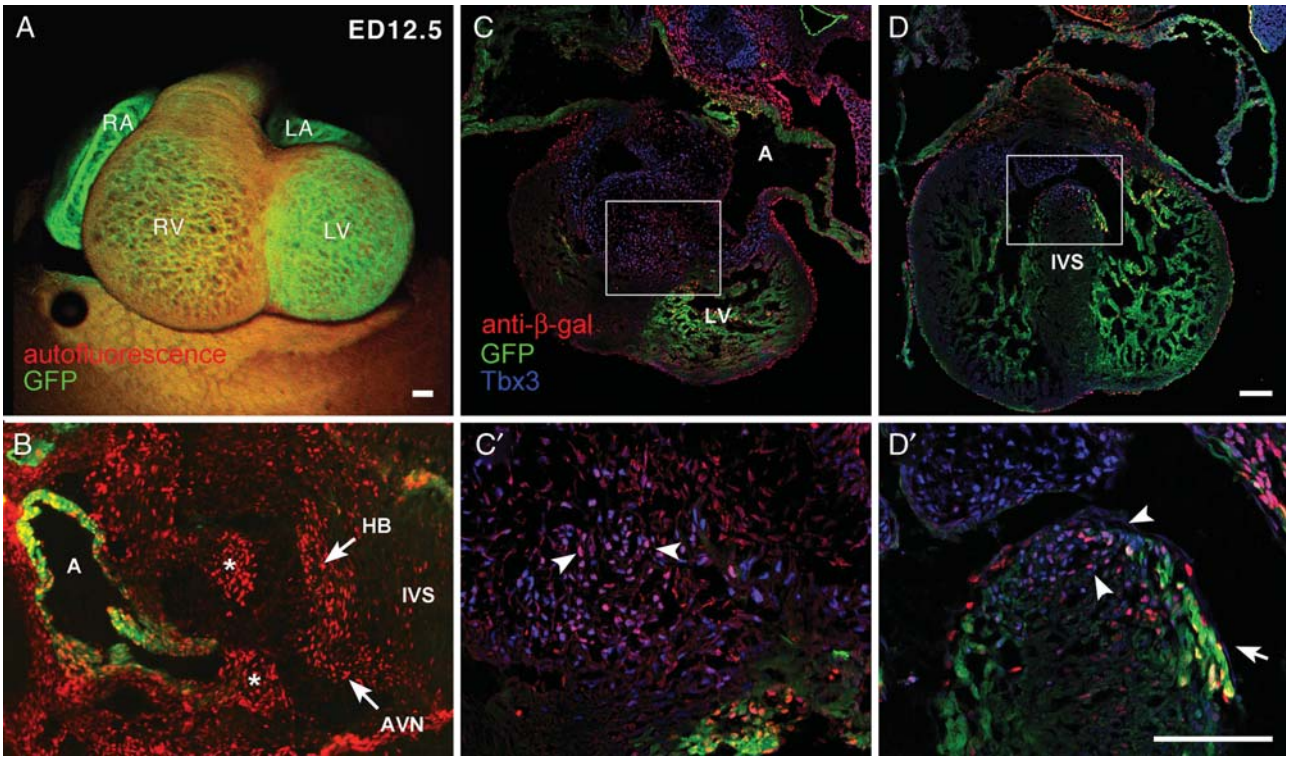

Figure 4 Heart structure and connection of the interventricular septum to atrioventricular node at ED12.5 in Cx40:GFP, T3-LacZ heterozygotes. (*A*) Whole-mount view depicts Cx40 expression in the heart; note stronger expression present in the left ventricle. Autofluorescence in red, GFP fluorescence in green. (*B*) Immunofluorescence staining on a sagittal section at the level of the interventricular septum (IVS). T3-lacZ detected in red is shown expressed at the level of the atrioventricular ring (*). It is also shown in a group of cells at the top of the interventricular septum (IVS) which corresponds to the His bundle (HB) connected to the dorsal atrioventricular node (AVN). (*C*, *C′*, *D*, *D′*) Immunofluorescence staining on transverse sections at the level of the atrioventricular node (*C*, *C′*) and His bundle (*D*, *D′*). In (*C*), Tbx3 immunostaining in blue highlights the AVN which cells also express the T3-lacZ transgene detected in red. (*C′*) corresponds to the high magnification of the AVN region boxed in (C) and showing Tbx3 and T3-LacZ both expressed in the same cells of the node (arrowheads). In (*D*), Cx40:GFP is detected in ventricular trabeculae of both ventricles while Tbx3 is detected in the mesenchymal cells of the cardiac cushion as wells as in the His bundle which covers the top of the IVS. Red cells expressing T3-lacZ transgene are also detected at the level of the His bundle. (*D′*) corresponds to the high magnification of this region boxed in (*D*) and showing Tbx3 and T3-LacZ both expressed in the same cells of the His bundle (arrowheads). The bundle branches express Cx40:GFP as well as Tbx3 and T3-LacZ (arrow). Scale bars 500 μm. LA, left atrium; LV, left ventricle; RA, right atrium; RV, right ventricle.

The ventricular activation pattern depends on the connection of the intraventricular conduction pathways to the atrioventricular node. The specificity of these connections as part of the atrioventricular conduction axis was verified by the Cx40:GFP marker (fast-conducting ventricular component, *Figure 4A*) and anti-β-galactosidase staining (T3-lacZ transgene labelling PIR tissues). At ED12.5, colocalization of these markers was observed at the proximal part of the bundle branches (*Figure 4D* and *D′*). The Tbx3 antibody labelled cells of the atrioventricular conduction system as well as the atrioventricular cushions (*Figure 4B–D*). Histological sectioning in the sagittal plane revealed the continuity of conduction markers between the atrial myocardium, atrioventricular canal, and the interventricular septum ventrally and dorsally (*Figure 4B*), consistent with the activation maps.

3.3 Calculation of left ventricular activation times

The left ventricular activation time showed a U-shaped relationship with development. It dropped to one-third between ED9.5–12.5, then stayed rather flat to increase slightly at later foetal stages (ED16.5 and ED18.5, *Figure 5A*). This suggests, however, continued increase in conduction velocity as the heart continues to increase in size (*Figure 3*). The shortest left ventricular activation time was recorded at ED13.5 (2.97 ± 0.83 ms) and was therefore used as a reference in statistical testing. No significant difference in activation time duration was observed between ED12.5–ED14.5, whereas it was significant ($P = 0.001$) at ED11.5 and highly significant ($P < 10^{-10}$) in the remaining embryonic days (ED9.5, 10.5, 16.5, 18.5, *Figure 5A*).

To discern whether the ventricular activation pattern has an influence on activation time and thus potential functional consequences, we performed a sub-analysis of ventricular activation times between ED9.5–ED11.5, where activation from the PIR was present. At all time points, activation from apical breakthrough resulted in shorter left ventricular activation time compared with activation through the PIR (*Figure 5B*). This difference reached statistical significance ($P = 0.005$) at ED10.5 and ED11.5.

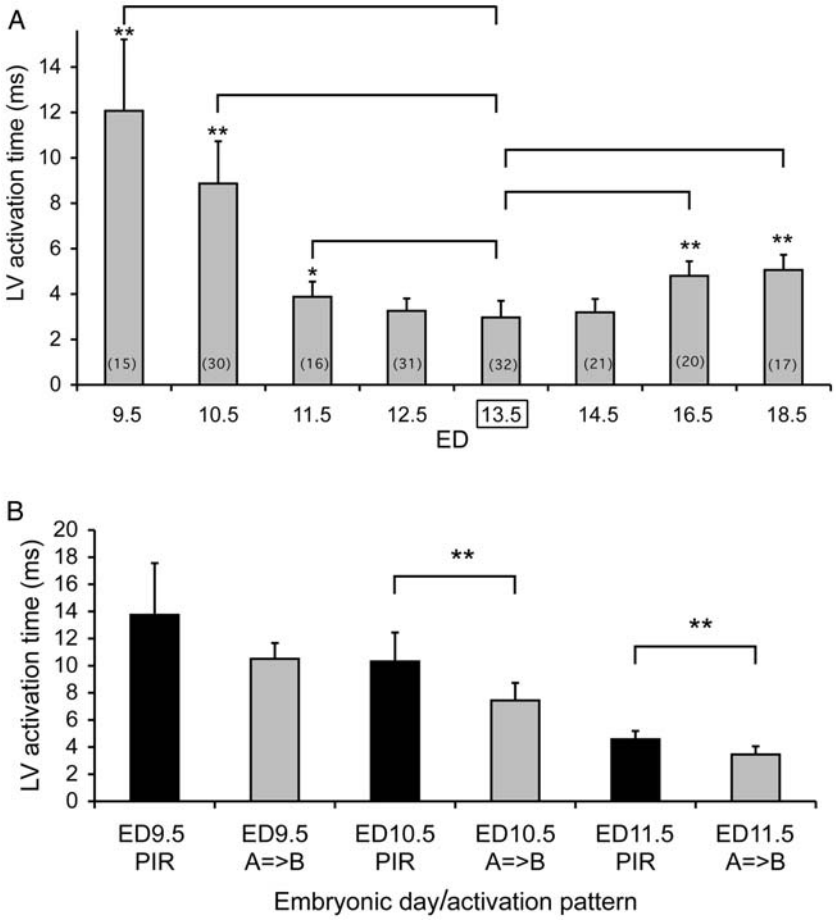

Figure 5 Quantification of ventricular conduction system maturation in *Cx40:GFP* heterozygotes. (*A*) Average time of left ventricular epicardial activation shows a U-shaped relationship with the development. The shortest activation time was found at ED13.5; against this stage were tested the remaining groups by unpaired two-tailed Student's *t*-test. The values are mean ± SD. $*P < 0.001$, $**P < 10^{-10}$. (*B*) The dependence of ventricular activation time duration on the activation pattern. Activation through the primary interventricular ring (PIR) is consistently slower than through the ventricular trabeculae (apex-to-base, A=>B). The *P*-value obtained with an unpaired two-tailed Student's *t*-test $**P < 0.005$. The values are mean ± SD.

3.4 Conduction changes in Cx40-deficient mice

There were no obvious differences in the frequency of the ventricular activation patterns between Cx40 null and control hearts at ED10.5 (data not shown) or ED12.5 (*Figure 6*). Interestingly, there was a notable decrease in the frequency of the left-sided apical breakthrough at ED12.5 and 14.5 in *Cx*40-deficient mice, with heterozygotes showing an intermediate phenotype. At these stages, however, the frequency of right-sided breakthrough was completely normal with no differences among genotypes (*Figure 6*). The resistance to right bundle branch block at ED14.5 could be correlated with *Cx*40 expression patterns in this region. Cx40 was initially expressed in a broad pattern (*Figure 7*), but during development became restricted to a thin strand of *Cx*40-positive tissue at ED18.5. The proportion of activation patterns began to reverse at ED16.5, where the left-sided breakthrough was present in nearly 100% in all genotypes (corresponding, at these stages, to functionality of the left bundle branch), while the frequency of the right-sided breakthrough began to decrease in the *Cx*40-deficient hearts, suggesting a developing right bundle branch dysfunction. These differences were even more prominent at ED18.5, where *Cx*40-deficient hearts presented only 33% of functional right bundle branches in contrast to 96% in heterozygotes and 94% in wild-type hearts (*Figure 6*). Quantitative analysis of left ventricle activation times performed at ED12.5–ED18.5 showed no differences between genotypes, including wild type vs. heterozygotes.

In a subset of hearts analysed at ED12.5, we observed a peculiar phenotype consisting of small ventricles with an elongated outflow tract, suggestive of abnormal morphogenesis described earlier[37] and consistent with a significantly less than 25% recovery rate for homozygous embryos in heterozygote crosses. The activation patterns of those morphologically abnormal hearts were not grossly disturbed (Supplementary material online, *Figure S1*), although the position of ventricular breakthroughs was slightly higher than in the control hearts.

4. Discussion

4.1 Conduction at early developmental stages

While a heartbeat was documented in mouse embryos as early as ED8.5 *in vivo* using ultrasound biomicroscopy,[38] we were able to

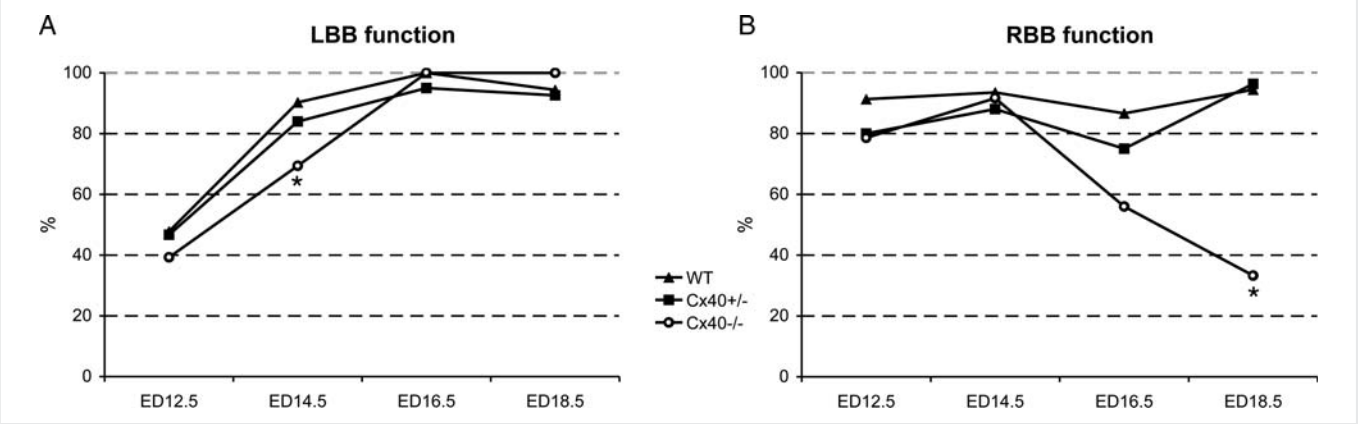

Figure 6 Conduction anomalies in *Cx*40-deficient embryonic ventricles. The frequency of the presence of left- and right-sided apical epicardial breakthroughs thought to correlate with the function of the left (LBB) and right bundle branch (RBB), respectively. Note that there is a left-sided deficiency initially (left panel) that is fully compensated by ED16.5, at which time point there is a clear decrease in the right-sided breakthrough frequency (right panel) corresponding to developing right bundle branch block. The heterozygotes show an intermediate phenotype. $*P < 0.05$ vs. wild type (as well as vs. heterozygotes for RBB at ED18.5); the difference between wild type and heterozygous animals was not significant.

obtain reproducible recordings only from ED9.5 onward using optical mapping. This could be due to the phototoxicity of the voltage sensitive dye, or generally higher sensitivity of mouse embryos compared with rats, in which similar recordings were obtained from the earliest stages of cardiac development by Hirota *et al.*[39] Their study described the location of the pacemaking tissue in the inflow region and its shift from the initially left side to the right side, but did not elaborate further on ventricular activation patterns. Our study extends previous reports on functionality of the developing mouse cardiac conduction system[7,8] by providing a quantification of the relative frequency of different activation patterns with appreciation of natural variability. Rentschler and associates quoted a small number of analysed hearts per group and concluded that only one activation pattern is typical at certain embryonic day. In the present study, we observed several activation patterns at each embryonic day, reflecting natural variability and consistent with the chick data.[2] Rentschler *et al.* described impulse propagation into the primitive ventricle along the dorsal wall only at ED9.5 (a pattern we interpret as an activation through the PIR), while our data show that the PIR can be recorded up to ED12.5. Moreover, activation from the apex of the primitive left ventricle towards the base in early embryonic development is a novel activation pattern at these stages.

A combination of functional recordings from a large number of hearts and both ventral and dorsal sides, together with our previous chick data,[3,5] changes our interpretation of the early activation patterns reported in the mouse by others[7,8] and in the rat by us.[10] Here, we show convincingly that the PIR, correlating with the forming interventricular groove,[6] is a specialized and preferred pathway used for ventricular activation. The PIR is composed of tissues around the interventricular foramen and part of the primary ring identified by Wessels *et al.*[6] Their description was based upon GlN2 expression in human samples: at stage 14 a ring around the interventricular foramen, but as the septation proceeded, GlN2 was expressed also in the right atrioventricular ring and the retroaortic root branch. In Aanhaanen *et al.*[40] as well as in *Figure 1*, the PIR is connected to the atrioventricular canal at two points, one ventral and one dorsal. The expansion of the atrioventricular canal towards right results in change in shape of the ring to a horseshoe, or U-shaped, structure. The ventral connection disappears later on, and only the dorsal node persists; otherwise, a dangerous arrhythmia (reciprocating tachycardia, as seen in Wolf–Parkinson–White syndrome) could result.

More discrete ring-shaped structures were described in the developing conduction system,[41] including the sinuatrial, atrioventricular, interventricular, and ventriculoarterial junctions using the minK-lacZ marker. While the expression of this marker changed with development, it provided developmental clues as to the possible origins of arrhythmias from regions outside the mature conduction system retaining expression of the marker. We believe that the PIR in our present work correlates well with the interventricular ring delineated by the minK-lacZ transgene at ED9.5. Multiple rings (3) were also described using the CCS-lacZ marker,[42] and again the connection between the atrioventricular canal and the 'primary ring' corresponds well with our observations (PIR, *Figure 1*). While the CCS-lacZ marker has the relative advantage of labelling the entire conduction system, further refinement is provided by using specific markers for slow (Tbx3, T3-lacZ transgene) and rapid (Cx40) conducting domains, allowing better appreciation of the connections between them.

Definitive connection between the atrial and ventricular myocardium through the atrioventricular node and His bundle occurs along the interatrial and ultimately fully fibrous atrioventricular septum. Hence, the atrial and ventricular septation process needs to be taken into consideration.[43] While the mature pattern of ventricular activation is present well before completion of ventricular septation, the role of atrial septum is less clear. It presents the shortest pathway between the sinoatrial and atrioventricular node, but it also forms a 'sink' slowing the propagation of the activation wave between the right and left atria.[44] Due to small size and delicacy of these structures during development, detailed analysis of conduction through this region would be challenging. While it is clearly part of the preferential atrioventricular conduction axis, experimental studies demonstrated functional pathways in the lateral region of the atrioventricular junction (Figure 5 in ref.[42]).

Conduction of electrical impulse through the PIR pathway is highly anisotropic (as can be appreciated from the shape of the isochrones)

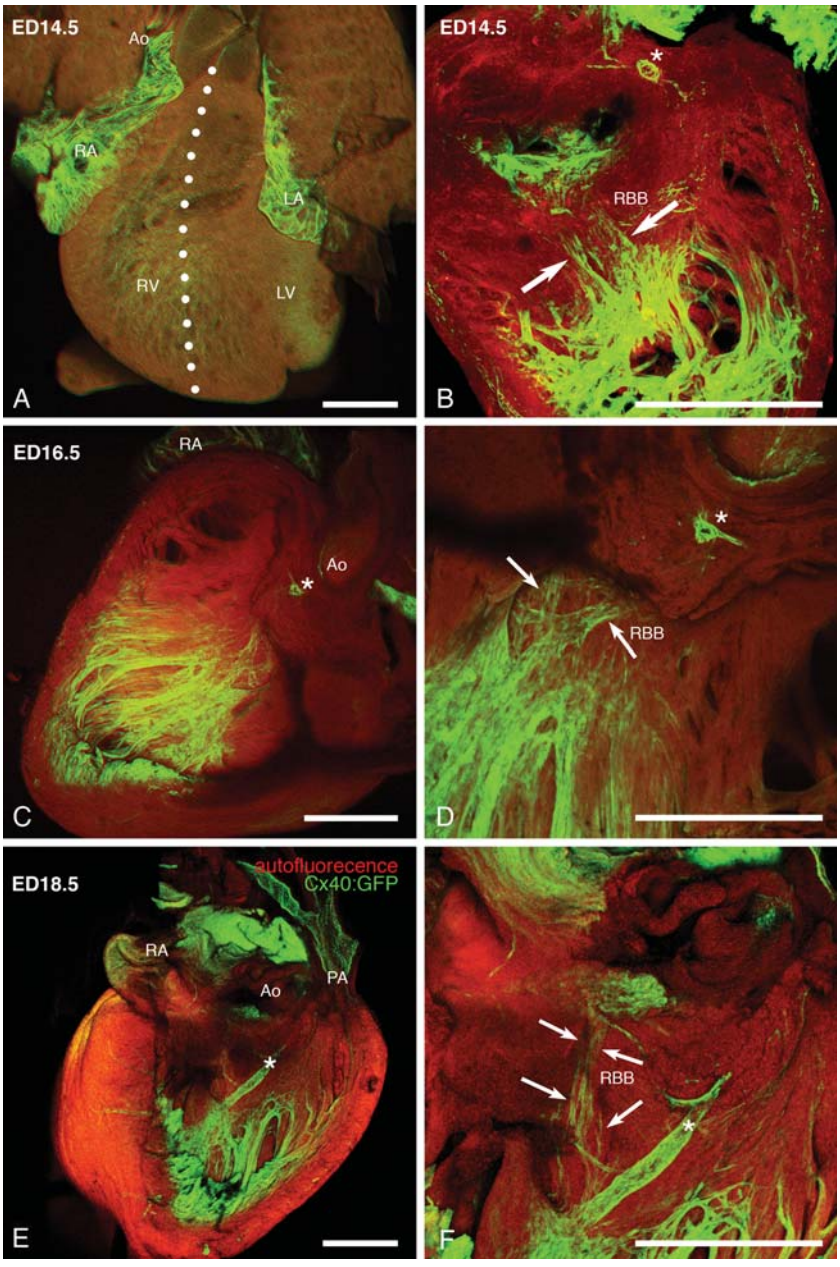

Figure 7 The development of the right bundle branch in *Cx40:GFP* heterozygotes. White dots indicate the line of right ventricle dissection to visualize the interventricular septum from the right side. The right bundle branch (RBB) is at ED14.5 a wide region of Cx40-positive fibres (marked laterally with arrows). *Cx*40 expression becomes restricted during later stages, resulting in the emergence of a thin strand of RBB at ED18.5. Asterisks indicate the septal artery, which is always near the RBB. Autofluorescence is in red and GFP fluorescence in green. Scale bars 500 μm. Ao, aorta; LA, left atrium; LV, left ventricle; PA, pulmonary artery; Pu, pulmonary trunk; RA, right atrium; RBB, right bundle branch; RV, right ventricle.

and slower than through the ventricular trabeculae forming the nascent definitive ventricular conduction system (*Figure 5B*). The differences in activation patterns between ED9.5 and 11.5 may potentially be due to ongoing cellular contribution from the second heart field, especially to the still forming right ventricle, which is complete at ED10.5. While the expression of *Cx*40 in right ventricular trabeculae is detectable already at ED10.5, activation from the right apical site was not observed until 1 day later, possibly because of the lack of connection of this expression domain with the preferential activation pathway utilizing the PIR and, much earlier, the left ventricular trabecular network.

*Cx*40-expressing trabeculae constitute the rapid conducting preferential pathway. In the left ventricle, Cx40 expression starts from ED9.5, and is always stronger than in the right ventricle. The functional consequence is demonstrated by sub-analysis of the activation time difference at stages where both conduction through the PIR and the more mature pathway utilizing the trabecular network, manifested as the apical breakthrough site, co-existed. In all cases, the activation through the trabecular network resulted in shorter ventricular activation time compared with the PIR (*Figure 5B*). A mature activation pattern from apex to base is connected with faster epicardial

activation time, which we consider, from the functional point of view, to be advantageous for efficient ventricular contraction. We postulate that such shorter epicardial activation time reflects a shorter ventricular activation time.

4.2 Conduction in later developmental stages and changes in Cx40-deficient mice

While the *Cx*40 is expressed in almost the entire trabecular network even at ED14.5 (*Figure* 7*A* and *B*) when the apical breakthrough sites suggest functionality of both bundle branches, not all trabeculae contribute to a definitive His-Purkinje network. Some will end up incorporated into the compact myocardium.[45] Pronounced left–right asymmetry, characteristic of the mature system[18] and resulting from gradual restriction of *Cx*40 expression, becomes apparent from ED18.5. This restriction, resulting in the emergence of a thin strand of *Cx*40-positive right bundle branch (*Figure* 7*E* and *F*), correlates with the time point at which right bundle branch block develops in Cx40-deficient embryos.

The data from Cx40 null mice suggest that while the function of the early ventricular conduction system is not strictly dependent upon the presence of *Cx*40 (as the PIR area is devoid of its expression), its later expression in the trabeculated chamber myocardium is important for the establishment of the preferential pathway through the trabecular network that will organize into the left and right bundle branches. The emergence of this pathway is manifested by the appearance of left and right apical epicardial breakthroughs in the spatiotemporal activation maps. We propose that tissue geometry is also of considerable importance for the function of the early conduction system. In the case of the developing right bundle branch in *Cx40*-deficient hearts, its function is initially normal and compensated by its relatively broad single-strand morphology until later stages, when increasing conduction velocity puts greater demands on the electrical coupling within specialized conduction fascicles. This correlates with the expression of *Cx*40 in right ventricular trabeculae starting 1 day before the appearance of the right apical breakthrough site. Indeed, conduction system morphology is normal in those hearts, and the right bundle branch block phenotype is fully penetrant only after birth.[22,23,25] Recently, right bundle branch block was reported in Irx3 null mice,[46] indicating higher sensitivity of this ventricular conduction system component to perturbations. On the other hand, high levels of expression of *Cx*40 in the left ventricular trabeculae seems to be more functionally relevant, as the diffuse conduction network, while providing a remarkable safety element, needs to be supplemented by appropriate electrical coupling for normal function. At this early stage, Cx43 is expressed in a similar pattern to Cx40, with a delay of 1 day. Cx40 is not expressed in the interventricular septum or the developing His bundle and its branches before ED14.5. The loss of Cx40 resulted in delayed left bundle branch functionality manifested initially as decreased frequency of the left-sided breakthrough, with tissue geometry (plus other conduction determinants, such as ion channel expression and other connexins) compensating only at later foetal stages (*Figure* 6).

4.3 Implications for future studies

Comparison of our wild-type data from different strains and background showed very little, if any, difference in frequency of ventricular activation patterns. Similarly, left ventricular activation times were not different between wild-type animals and Cx40 heterozygotes, suggesting that our data could be used as a baseline for analysis of other mutants. The variable that should be controlled is the crown rump length, as this varies among litters even with the same gestational age. Quantitative analysis of normal mouse embryonic ventricular conduction patterns will thus be useful for the interpretation of effects of mutations affecting the function of the cardiac conduction system. Additional topic worth of further investigation is the fate of the components of the atrioventricular ring as well as the interatrial septum in the final production of an atrioventricular node, and the details of its connections with the ventricular conduction system.

Supplementary material

Supplementary material is available at *Cardiovascular Research* online.

Acknowledgements

We would like to thank Ms Marie Jindrakova, Ms Jarmila Svatunkova, and Ms Eva Kluzakova for excellent technical assistance. The kind assistance of Dr Robert Kelly (IBDML, Marseille) with language revision is highly appreciated.

Conflict of interest: none declared.

Funding

This work was supported by the Ministry of Education VZ 0021620806, LC06044, and PRVOUK-P35/LF1/5; Academy of Sciences Purkinje Fellowship to D.S., and institutional AV0Z50110509 and RVO: 67985823. J.B. and B.S. were supported by the Graduate student training program of the First Faculty of Medicine, Charles University in Prague. Further support comes from the Grant Agency of the Czech Republic 304/08/0615, 204/09/H084, and P302/11/1308 to D.S. and the AFM (Association Française contre les Myopathies) to L.M.

References

1. Chuck ET, Freeman DM, Watanabe M, Rosenbaum DS. Changing activation sequence in the embryonic chick heart. Implications for the development of the His-Purkinje system. *Circ Res* 1997;**81**:470–476.
2. Reckova M, Rosengarten C, deAlmeida A, Stanley CP, Wessels A, Gourdie RG *et al.* Hemodynamics is a key epigenetic factor in development of the cardiac conduction system. *Circ Res* 2003;**93**:77–85.
3. Sedmera D, Reckova M, Bigelow MR, DeAlmeida A, Stanley CP, Mikawa T *et al.* Developmental transitions in electrical activation patterns in chick embryonic heart. *Anat Rec* 2004;**280A**:1001–1009.
4. Chuck ET, Meyers K, France D, Creazzo TL, Morley GE. Transitions in ventricular activation revealed by two-dimensional optical mapping. *Anat Rec* 2004;**280A**: 990–1000.
5. Sankova B, Machalek J, Sedmera D. Effects of mechanical loading on early conduction system differentiation in the chick. *Am J Physiol Heart Circ Physiol* 2010;**298**: H1571–H1576.
6. Wessels A, Vermeulen JL, Verbeek FJ, Viragh S, Kalman F, Lamers WH *et al.* Spatial distribution of 'tissue-specific' antigens in the developing human heart and skeletal muscle. III. An immunohistochemical analysis of the distribution of the neural tissue antigen G1N2 in the embryonic heart; implications for the development of the atrioventricular conduction system. *Anat Rec* 1992;**232**:97–111.
7. Rentschler S, Vaidya DM, Tamaddon H, Degenhardt K, Sassoon D, Morley GE *et al.* Visualization and functional characterization of the developing murine cardiac conduction system. *Development* 2001;**128**:1785–1792.
8. Rentschler S, Zander J, Meyers K, France D, Levine R, Porter G *et al.* Neuregulin-1 promotes formation of the murine cardiac conduction system. *Proc Natl Acad Sci USA* 2002;**99**:10464–10469.
9. Rothenberg F, Nikolski V, Watanabe M, Efimov I. Electrophysiology and anatomy of embryonic rabbit hearts before and after septation. *Am J Physiol Heart Circ Physiol* 2005;**288**:H344–H351.
10. Sedmera D, Reckova M, Rosengarten C, Torres MI, Gourdie RG, Thompson RP. Optical mapping of electrical activation in developing heart. *Microscop Microanal* 2005;**11**:209–215.

11. Coppen SR, Severs NJ, Gourdie RG. Connexin45 (alpha 6) expression delineates an extended conduction system in the embryonic and mature rodent heart. *Dev Genet* 1999;**24**:82–90.
12. Kumai M, Nishii K, Nakamura K, Takeda N, Suzuki M, Shibata Y. Loss of connexin45 causes a cushion defect in early cardiogenesis. *Development* 2000;**127**:3501–3512.
13. Munshi NV, McAnally J, Bezprozvannaya S, Berry JM, Richardson JA, Hill JA *et al*. Cx30.2 enhancer analysis identifies Gata4 as a novel regulator of atrioventricular delay. *Development* 2009;**136**:2665–2674.
14. Gros D, Theveniau-Ruissy M, Bernard M, Calmels T, Kober F, Sohl G *et al*. Connexin 30 is expressed in the mouse sino-atrial node and modulates heart rate. *Cardiovasc Res* 2010;**85**:45–55.
15. Haugan K, Miyamoto T, Takeishi Y, Kubota I, Nakayama J, Shimojo H *et al*. Rotigaptide (ZP123) improves atrial conduction slowing in chronic volume overload-induced dilated atria. *Basic Clin Pharmacol Toxicol* 2006;**99**:71–79.
16. Severs NJ, Coppen SR, Dupont E, Yeh HI, Ko YS, Matsushita T. Gap junction alterations in human cardiac disease. *Cardiovasc Res* 2004;**62**:368–377.
17. Vaidya D, Tamaddon HS, Lo CW, Taffet SM, Delmar M, Morley GE *et al*. Null mutation of connexin43 causes slow propagation of ventricular activation in the late stages of mouse embryonic development. *Circ Res* 2001;**88**:1196–1202.
18. Miquerol L, Meysen S, Mangoni M, Bois P, van Rijen HV, Abran P *et al*. Architectural and functional asymmetry of the His-Purkinje system of the murine heart. *Cardiovasc Res* 2004;**63**:77–86.
19. Miquerol L, Moreno-Rascon N, Beyer S, Dupays L, Meilhac SM, Buckingham ME *et al*. Biphasic development of the Mammalian ventricular conduction system. *Circ Res* 2010; **107**:153–161.
20. van Kempen MJ, ten Velde I, Wessels A, Oosthoek PW, Gros D, Jongsma HJ *et al*. Differential connexin distribution accommodates cardiac function in different species. *Microsc Res Tech* 1995;**31**:420–436.
21. Leaf DE, Feig JE, Vasquez C, Riva PL, Yu C, Lader JM *et al*. Connexin40 imparts conduction heterogeneity to atrial tissue. *Circ Res* 2008;**103**:1001–1008.
22. Simon AM, Goodenough DA, Paul DL. Mice lacking connexin40 have cardiac conduction abnormalities characteristic of atrioventricular block and bundle branch block. *Curr Biol* 1998;**8**:295–298.
23. Tamaddon HS, Vaidya D, Simon AM, Paul DL, Jalife J, Morley GE. High-resolution optical mapping of the right bundle branch in connexin40 knockout mice reveals slow conduction in the specialized conduction system. *Circ Res* 2000;**87**:929–936.
24. Kirchhoff S, Nelles E, Hagendorff A, Kruger O, Traub O, Willecke K. Reduced cardiac conduction velocity and predisposition to arrhythmias in connexin40-deficient mice. *Curr Biol* 1998;**8**:299–302.
25. van Rijen HV, van Veen TA, van Kempen MJ, Wilms-Schopman FJ, Potse M, Krueger O *et al*. Impaired conduction in the bundle branches of mouse hearts lacking the gap junction protein connexin40. *Circulation* 2001;**103**:1591–1598.
26. Fedorov VV, Lozinsky IT, Sosunov EA, Anyukhovsky EP, Rosen MR, Balke CW *et al*. Application of blebbistatin as an excitation-contraction uncoupler for electrophysiologic study of rat and rabbit hearts. *Heart Rhythm* 2007;**4**:619–626.
27. Jou CJ, Spitzer KW, Tristani-Firouzi M. Blebbistatin effectively uncouples the excitation-contraction process in zebrafish embryonic heart. *Cell Physiol Biochem* 2011;**25**:419–424.
28. Sedmera D, Harris BS, Grant E, Zhang N, Jourdan J, Kurkova D *et al*. Cardiac expression patterns of endothelin-converting enzyme (ECE): implications for conduction system development. *Dev Dyn* 2008;**237**:1746–1753.
29. Nanka O, Krizova P, Fikrle M, Tuma M, Blaha M, Grim M *et al*. Abnormal myocardial and coronary vasculature development in experimental hypoxia. *Anat Rec (Hoboken)* 2008;**291**:1187–1199.
30. Viragh S, Challice CE. The development of the conduction system in the mouse embryo heart. I. The first embryonic A-V conduction pathway. *Dev Biol* 1977;**56**: 382–396.
31. Viragh S, Challice CE. The development of the conduction system in the mouse embryo heart. II. Histogenesis of the atrioventricular node and bundle. *Dev Biol* 1977;**56**:397–411.
32. Viragh S, Challice CE. The development of the conduction system in the mouse embryo heart. *Dev Biol* 1982;**89**:25–40.
33. Sedmera D, Reckova M, DeAlmeida A, Coppen SR, Kubalak SW, Gourdie RG *et al*. Spatiotemporal pattern of commitment to slowed proliferation in the embryonic mouse heart indicates progressive differentiation of the cardiac conduction system. *Anat Rec* 2003;**274A**:773–777.
34. Wessels A, Markman MW, Vermeulen JL, Anderson RH, Moorman AF, Lamers WH. The development of the atrioventricular junction in the human heart. *Circ Res* 1996; **78**:110–117.
35. Miquerol L, Dupays L, Theveniau-Ruissy M, Alcolea S, Jarry-Guichard T, Abran P *et al*. Gap junctional connexins in developing mouse cardiac conduction system. In: Goode J, eds. *Development of the Cardiac Conduction System*. Chichester: Wiley; 2003. p98–109.
36. Miller CE, Thompson RP, Bigelow MR, Gittinger G, Trusk TC, Sedmera D. Confocal imaging of the embryonic heart: How deep? *Microscop Microanal* 2005;**11**:216–223.
37. Kirchhoff S, Kim JS, Hagendorff A, Thonnissen E, Kruger O, Lamers WH *et al*. Abnormal cardiac conduction and morphogenesis in connexin40 and connexin43 double-deficient mice. *Circ Res* 2000;**87**:399–405.
38. Phoon CK. Imaging tools for the developmental biologist: ultrasound biomicroscopy of mouse embryonic development. *Pediatr Res* 2006;**60**:14–21.
39. Hirota A, Kamino K, Komuro H, Sakai T, Yada T. Early events in development of electrical activity and contraction in embryonic rat heart assessed by optical recording. *J Physiol* 1985;**369**:209–227.
40. Aanhaanen WT, Mommersteeg MT, Norden J, Wakker V, de Gier-de Vries C, Anderson RH *et al*. Developmental origin, growth, and three-dimensional architecture of the atrioventricular conduction axis of the mouse heart. *Circ Res* 2010;**107**:728–736.
41. Kondo RP, Anderson RH, Kupershmidt S, Roden DM, Evans SM. Development of the cardiac conduction system as delineated by minK-lacZ. *J Cardiovasc Electrophysiol* 2003; **14**:383–391.
42. Jongbloed MR, Wijffels MC, Schalij MJ, Blom NA, Poelmann RE, van der Laarse A *et al*. Development of the right ventricular inflow tract and moderator band: a possible morphological and functional explanation for Mahaim tachycardia. *Circ Res* 2005;**96**: 776–783.
43. Webb S, Brown NA, Anderson RH. Formation of the atrioventricular septal structures in the normal mouse. *Circ Res* 1998;**82**:645–656.
44. Sedmera D, Wessels A, Trusk TC, Thompson RP, Hewett KW, Gourdie RG. Changes in activation sequence of embryonic chick atria correlate with developing myocardial architecture. *Am J Physiol Heart Circ Physiol* 2006;**291**:H1646–H1652.
45. Sedmera D, Pexieder T, Vuillemin M, Thompson RP, Anderson RH. Developmental patterning of the myocardium. *Anat Rec* 2000;**258**:319–337.
46. Zhang SS, Kim KH, Rosen A, Smyth JW, Sakuma R, Delgado-Olguin P *et al*. Iroquois homeobox gene 3 establishes fast conduction in the cardiac His-Purkinje network. *Proc Natl Acad Sci USA* 2011;**108**:13576–13581.